The Impacts of Freeze-thaw Cycles on Saturated Hydraulic Conductivity and Microstructure of Saline-alkali Soils

Wenshuo Xu
Shandong Agricultural University
Kesheng Li
Shandong Agricultural University
Longxiao Chen
Shandong Agricultural University
Weihang Kong
Shandong Agricultural University
Chuanxiao Liu (lchuanx@163.com)
Shandong Agricultural University

Research Article

Keywords: Saline-alkali soil, Freeze-thaw cycle, Saturated hydraulic conductivity, MIP Dry densities, Water content

Posted Date: June 30th, 2021

DOI: https://doi.org/10.21203/rs.3.rs-654374/v1

The impacts of freeze-thaw cycles on saturated hydraulic conductivity and microstructure of saline-alkali soils

Wenshuo Xu Kesheng Li Longxiao Chen Weihang Kong Chuanxiao Liu*

[1]College of Water Conservancy and Civil Engineering, Shandong Agricultural University, Tai'an 271018, Shandong, China.

*Corresponding author: Chuanxiao Liu.

Abstract: Study on the microscopic structure of saline-alkali soil can reveal the change of its permeability more deeply. In this paper, the relationship between permeability and microstructure of saline-alkali soil with different dry densities and water content in the floodplain of southwestern Shandong Province was studied through freeze-thaw cycles. A comprehensive analysis of soil samples was conducted using particle-size distribution, X-Ray diffraction, Freeze-Thaw cycle test, saturated hydraulic conductivity test and mercury intrusion porosimetry. The poor microstructure of soil is the main factor that leads to the category of micro-permeable soil. The porosity of the local soil was only 6.19-11.51%, and ultra-micropores (<0.05 μm) and micropores (0.05-2 μm) dominated the pore size distribution. Soil saturated water conductivity was closely related to its microscopic pore size distribution. As the F-T cycles progressed, soil permeability became stronger, with the reason the pore size distribution curve began to shift to the small pores (2-10 μm) and mesopores (10-20 μm), and this effect was the most severe when the freeze-thaw cycle was 15 times. High water content could promote the effects of freeze-thaw cycles on soil permeability and pore size distribution, while the increase of dry density could inhibit these effects. The results of this study provide a theoretical basis for the remediation of saline-alkali soil in the flooded area of Southwest Shandong.

Keywords: Saline-alkali soil Freeze-thaw cycle Saturated hydraulic conductivity MIP Dry densities Water content.

1. Introduction

The problem of soil salinization is distributed in more than 100 countries and regions around the world. At present, the salinized soil has reached 1 billion hectares in the world and is gradually increasing every year[1-2]. Soil salinization will impoverish the land, which is not conducive to the health maintenance of the local ecosystem[3], leading to low agricultural production capacity[4-5], which has become one of the major problems restricting the development of global agricultural production and environmental construction. Studies have shown that soil salinization is essentially soil degradation, which will increase soil bulk density and electrical conductivity, and reduce soil permeability and water retention capacity[6-7]. On this basis, in order to improve this bad property, the current improvement methods are generally accepted to add desulfurization gypsum, biomass charcoal and fly ash to the saline-alkali soil[8-11]. However, the problems of cost control and environmental pollution cannot be ignored[12-13]. In order to explore a new idea of saline-alkali soil improvement, our study is devoted to studying the relationship between soil microstructure and its physical properties (this paper mainly refers to soil permeability) after F-T cycles.

At present, there are about 340,000 km^2 of saline-alkali land in China, accounting for 25.2% of the country's arable land area. These saline-alkali lands are mainly distributed in northern China, especially in the Yellow River Basin[14]. The Yellow River floodplain in the southwest of Shandong Province in China is a seasonal permafrost region. The saline-alkali land in this region is scattered and widely distributed, covering an area of more than 163 km^2, accounting for 45.96% of the unused land[15]. The region

relies mainly on water conservancy measures to control the saline-alkali land, but because of its inland location, fresh water resources are scarce. Although the people in this area has been improving the saline-alkali land with straw returning method, the effect is still far from enough. Thus, it is urgent to develop a new saline-alkali land improvement measure.

Many scholars have proved that there is a close relationship between the physical properties and microstructure of soils[16-19] analyzed the connection mode of particles in the skeleton of salinized soil and found that the cement of salt crystals in the skeleton would affect the mechanical strength of salinized soil. Zhang et al.[20] by means of SEM, MIP and NA to conduct a complete qualitative and quantitative evaluation of the pore characteristics of clay in coastal areas, and found that the colloid bonding and disordered open flocculating structure of the clay in Zhanjiang area contributed to the poor physical and mechanical properties of the clay in this area. Jha and Sivapullaiah[21] studied the microstructure of clay by SEM and analyzed the physical properties of lime treated montmorillonite. In addition, as one of the physical properties of soil, soil water permeability is used to characterize soil permeability and internal pore characteristics, and it is an important parameter in agricultural irrigation[22-23]. It has been proved that the microstructure of saline-alkali soil is closely related to its physical properties, especially its permeability[24-25]. Therefore, in the field of civil engineering, soil microstructure has gradually become one of the criteria for determining soil physical properties. However, researches mainly focus on loess and clay, and researches in the field of saline-alkali soil are relatively scarce. Therefore, the researches on the

71 microstructure of saline-alkali soil can provide a new idea for the restoration of such
72 degraded soil.

73 Recently, many scholars have found that F-T cycles can lead to changes in soil
74 physical properties and microstructure. For unsaturated dispersed soils with different
75 salinity, the F-T cycles could change their instantaneous water conductivity and matric
76 suction, and the effects were not monotonic with the increase of the number of F-T
77 cycles[26]. F-T cycles increased soil porosity and saturated water conductivity, change
78 soil physical properties, and there is at least one cycle time threshold (between 5 and
79 20 cycles)[27]. Liu et al.[28] found that the freeze-thaw cycles would destroy the coarse
80 particles in lime solidified saline-alkali soil, collect fine particles and increase the
81 diameter of macropores. Moreover, many researchers have studied the relationship
82 between F-T cycles and soil permeability, and it is believed that dry density and water
83 content are important factors affecting freeze-thaw cycles[29-30]. Meanwhile, the previous
84 studies on soil after F-T cycles mostly focused on its mechanical properties and mostly
85 qualitative research[31-32]. However, there are no comprehensive studies on the
86 permeability and microstructure of saline-alkali soil in the southwest of Shandong
87 Province after freeze-thaw cycles.

88 Inspired by the above studies, PSD analysis, XRD analysis, freeze-thaw cycle test,
89 saturated hydraulic conductivity test and MIP analysis were performed on the saline-
90 alkali soil remolded according to different dry densities and water content in the flooded
91 area of Southwest Shandong Province. The objective of this study is to determine the
92 saturated hydraulic conductivity and microscopic pore size distribution of saline-alkali

soil in the floodplain of Southwest Shandong Province after F-T cycles. It is expected to find the relationship between the microstructure and permeability of the saline-alkali soil in this area, so as provide a new theoretical basis for its treatment.

2. Materials and methods

2.1. Experimental materials

The test soil samples were collected in He-ze City, Shandong Province, which is located in the Yellow River Basin at an altitude of 50 m in the southwest of Shandong Province, and is a typical Yellow River flooding area in Shandong Province. Its region has a warm temperate monsoon continental climate with strong seasonality in temperature, rainfall, wind and evaporation. The average annual temperature in this region is 13.7 °C, the extreme minimum temperature is -16.5 °C, and the extreme maximum temperature is 40.5 °C. It belongs to the seasonal frozen soil region. The annual frost-free period is 210 days, and the annual average precipitation is 625 mm, which is concentrated in June to September. The annual average wind speed is 1.95 m/s, and the average wind speed from January to April is 2.33 m/s. The annual average evaporation is 874.82 mm, the maximum value appears in June, and the minimum value appears in January. The area is inland and lacks fresh water, so the Yellow River is the only source of irrigation water.

The local soil was severely damaged by salt, and its $EC_{1:5}$ reached 1.44 dS m^{-1}, PH<8.5, belonging to weakly alkaline soil. At the same time, exchange sodium percentage (ESP) reaches 31.14%, far more than 15%, so these poor soils are usually classified as "saline-alkali soil" (Table 1). The accumulation of salt, especially

115 excessive Na^+, led to the deterioration of soil properties in this area, with a salt content
116 of 61.96 g kg^{-1}. The K_s of the soil in this area was only 1.48×10^{-5} cm/s, which belongs
117 in the micro-permeable water class according to the code for engineering geological
118 investigation of water resources and hydropower[33].

119 Soil samples were collected from the vicinity of Dongming County, He-ze City,
120 Shandong Province, located at 115.08°E, 35.38°N (Fig. 1). A number of undisturbed
121 soil samples and scattered soil samples were taken from the test site for later
122 measurement of the basic physical properties of the soil and preparation of soil samples
123 for subsequent experiments. The clay (<0.002 mm) in the soil samples is 4.95%, and
124 the silt (0.002-0.02 mm) is 42.90%, sand (>0.02 mm) in soil, reaching 52.15%. The soil
125 texture of this region can therefore be classified as silty clay. Other basic
126 physicochemical properties of the soil in this area are shown in Table 1.

127 **2.2. Preparation of specimens**

128 A small number of soil samples were dried at 105°C, crushed and sifted through
129 75 μm for PSD and XRD analysis. The other samples were air-dried, rolled and crushed
130 and passed through a 2 mm sieve. The F-T cycles (N) of 0, 1, 5, 10, 15, 20 were set.
131 The water content was 13%, 16%, 19%, and the dry density of remolded soil was 1.48
132 g cm^{-3}, 153 g cm^{-3}, 1.58 g cm^{-3}, a total of 54 groups of samples (Table 2). The remolded
133 sample were left in the shade for 24 hours to ensure sufficient moisture diffusion. Then,
134 the 77 × 40 mm soil sample was prepared by electrohydraulic demodding mechanism.
135 The 61.8 × 40 mm ring knifes coated with Vaseline were used to cut the sample and
136 wrap the plastic film for F-T cycle test and saturated hydraulic conductivity test. At the

end of the above tests, we gently removed the soil samples from the ring knifes and prepare the test samples for MIP analysis according to the liquid nitrogen vacuum freeze-drying method[34-35]. The soil samples were cut into 5 × 5 × 10 mm cubes for MIP analysis.

2.3. Particle size distribution and X-ray diffraction before F-T cycles

The PSD analysis of soil can facilitate us to understand the composition of soil particles and the uniformity of particle size distribution. The BT-9300S laser particle analyzer (Dandong Baite Instrument Co., Ltd., Dandong City, China) was used to complete soil PSD analysis, and two grading indexes were used to analyze the uniformity of soil particles, namely uniformity coefficient (C_u) and curvature coefficient (C_c). Uniformity coefficient is used to reflect the distribution of different particle groups, and C_c is used to judge the continuity of slope of cumulative curve of soil particle size distribution, and it is also an important index to judge whether soil particle size distribution is good. The expressions are as follows:

$$C_u = \frac{d_{60}}{d_{10}} \quad (1)$$

$$C_c = \frac{d_{30}^2}{d_{10} \times d_{60}} \quad (2)$$

Where d_{10} is effective grain size, d_{30} is median grain size, and d_{60} is control grain size. d_{10}，d_{30}，d_{60} represent the percentage of particles of the corresponding size that are 10%, 30%, and 60% smaller than the sample.

The mineral composition of soil affects the physical and chemical properties of

157 soil[36-37], which we analyzed using a TD-3500 X-ray diffractometer (Dandong Tongda
158 Technology Co., Ltd., Dandong City, China).

159 **2.4. Freeze-thaw cycling experiments**

160 Freezing and thawing will change the physical properties and internal structure[38]
161 of soil. F-T tests were carried out in a closed system and no moisture was supplied to
162 the sample during the test for providing conditions similar to field conditions[39]. In this
163 study, the freeze-thaw cycles were split into six: the initial state (no cycle) and sets
164 ending after the 1st, 5rd, 10th, 15th and 20th cycle. The soil samples were subjected to
165 a freezing temperature of −15 °C for 12 h in order to obtain complete frost penetration.
166 After freezing, they were allowed to thaw at a room temperature of about 10 °C for 12
167 h before being subjected to the next cycle. An Ultra-low temperature refrigerated
168 storage tank (DW-HL290) manufactured by Zhongke Meiling Cryogenics Co., Ltd was
169 used for this purpose. On the basis of no more than 0.5°C error, the refrigerated storage
170 tank has a temperature adjustment range of −5 °C to −87°C and the temperature is
171 visible.

172 **2.5. Saturated hydraulic conductivity**

173 Saturated hydraulic conductivity (K_s) represents the upper limit of water migration rate
174 for soil, and it is one of the crucial hydraulic properties of soil[40]. Soil permeability is
175 closely related to its microstructure[41]. In this study, According to the code for
176 geotechnical testing[42], variable head osmotic apparatus (TST-55) was carried out the
177 SHC test of soil. Before the test, the soil samples were placed in a vacuum saturator
178 for 24 h to ensure that the soil samples reached the saturation state. The flow rate was

179 measured under the condition of variable head. Considering the effect of temperature
180 on water viscosity, the water temperature was monitored in real time during the test.
181 The expression of K_s is as follows[43]:

182 $$K_s = \frac{aL}{At} ln \frac{h_1}{h_2} \quad (3)$$

183 Where K_s is the saturated hydraulic conductivity (cm s^{-1}), a is the cross-sectional
184 area of the standpipe (m^2), L is the length of the sample (m), A is the cross-sectional
185 area of the sample (m^2), h_1 and h_2 are the initial and final water head with respect to the
186 outflow (m) and t is the time for the hydraulic head difference to decrease from h_1 to h_2.

187 **2.6. Mercury intrusion porosimetry**

188 MIP is a relatively straightforward method, which can be used to derive the values of
189 other important characteristic parameters, including total porosity, average pore
190 diameter, median pore diameter, and most probable pore diameter, and the measured
191 pore diameters range from 7nm to 350 μm.

192 In present study, we measured soil porosity and pore size distribution using MIP.
193 Pre-lyophilized MIP samples were directly used for the MIP analysis, we used a fully
194 automatic PM-33-18 mercury intrusion analyzer (Conta Instruments Company, US).
195 Mercury will be injected into the soil sample under a certain degree of pressure.
196 Therefore, according to the pressure applied to mercury and the volume of mercury
197 invasion, the pore distribution of the soil sample can be obtained through the Washburn
198 equation[44]. The expression is as follows:

$$p = -\frac{2\sigma \cos\theta}{r} \quad (4)$$

Where P is the applied pressure, σ is the surface tension coefficient of the immersed liquid, θ is the contact angle between liquid and solid materials, and r is the cylindrical pore radius. Among them, the values of σ and θ were 0.485 N m^{-1} and 140° in this study, respectively[45].

Soil pores can be classified into inactive pores, capillary pores and aerated pores according to their function and size. The porosity of the inactive pore is less than 2 μm, and the permeability is the worst. As the diameter increases, the permeability of pores becomes better[20]. In order to facilitate the pore size classification of saline-alkali soil in the Yellow River floodplain of Southwest Shandong, China. Our study based on the Shear pore size division theory[46], and other scholars[47-48], combining with the pore characteristics of the local saline-alkali soil (Table 3) to divide the pore size of saline-alkali soil in this area.

3. Results

3.1. Quantitative analysis of the mineral phase and PSD

It is found that the particle size of saline-alkali soil in this area is in the range of 1 to 100 μm, and the particle density curve was unimodal (Fig. 2). The relevant soil characteristic parameters in this area, C_u=7.14, C_c=0.33. According to the regulations of the Ministry of Water Resources of the People's Republic of China[33], C_u>5, the distribution of soil grain size is not uniform. C_c<1, indicating that the soil is dominated by small particles. From this, we can preliminarily judge that the grain size distribution

220 of saline-alkali soil in this area is poor, leading to its poor permeability.

221 Figure 2 shows the XRD map of the saline-alkali soil in this area. Table 4 shows
222 the mineral composition of the local saline-alkali soil. The mineral composition of the
223 soil includes quartz, albite, orthoclase, calcite, kaolinite, illite and chlorite. Primary
224 minerals account for more than 90% of the total minerals, and quartz is the highest,
225 accounting for 51.85% of the total minerals, followed by albite and calcite. Clay
226 minerals (kaolinite, illite, chlorite) only accounted for 9.55% of the total mineral
227 content of the soil, among which illite was dominant, reaching 5.68% of the total
228 mineral content of the soil.

229 **3.2. Surface fragmentation of soil samples after F-T cycles**

230 In this study, in order to better observe the macroscopic effects of freeze-thaw
231 cycles on soil, we selected several representative experimental groups to demonstrate.
232 Fig. 3 shows soil samples with a water content of 13%, 1.48 g cm^{-3} and different freeze-
233 thaw cycles. With the increase of the number of freeze-thaw cycles, we found that the
234 surface fragmentation of soil samples from A1 to F1 was more and more obvious. By
235 observing F1-F3 (Fig. 4), it is found that under the same number of freeze-thaw cycles
236 and dry density, high water content can make the surface of soil samples more broken.
237 However, the change of dry density of a single factor has no obvious influence on the
238 surface macrophenomena of soil samples (Fig. 4).

239 **3.3. Saturated hydraulic conductivity after F-T cycles**

240 Fig. 5 summarizes the changes of *Ks* of water-bearing remolded soil caused by the
241 changes of F-T cycles. Under the three dry densities of 1.48, 1.53 and 1.58 g cm^{-3}, the

soil K_s increased with the increase of the number of cycles and reached the threshold value at N=15, and then showed a decreasing trend. Taking 1.48 g cm^{-3} as an example, when N=15, the K_s of the three water contents of soil samples increased by 260.95%, 270.95% and 283.33%, respectively. We found that after the first cycle, the increment of K_s decreased with the change of the cycle. Nevertheless, the increment of the first cycle was the largest, which might be because the freeze-thaw cycle affected the development of soil pores. Fig. 6 shows the changes of K_s with water content of water-remolded soil. F-T cycle (N=0) before and after freezing and thawing cycle of soil samples have significant differences, the F-T cycle before the K_s is hardly affected by the water content change, K_s of soil after freezing and thawing cycle had approximate linear relationship with the increase of water content, the F-T cycle test with us observed is consistent with the regular pattern of soil sample surface broken. However, The soil water content increased from 13% to 19%, and the K_s increased relatively little. Under the three dry densities, the maximum elevation was 31.68%, 18.91% and 32.63% respectively. At the same time, we found that the K_s of soil samples would be enhanced as long as they experienced F-T cycles, which indicated that F-T cycles would have an impact on soil structure.

The relationship between K_s and dry density of water-bearing remolded saline-alkali soil is shown in Fig. 7. When the soil dry density is high, the K_s decreases significantly, but the attenuation rate decreases. The higher the dry density of the soil, the higher the degree of internal consolidation of the soil, which will affect the pores in the soil, resulting in compression or even closure, thus blocking the seepage channel.

In addition, we found that compared with the F-T cycles of 20 times (N=20) and 10 times (N=10), with the increase of dry density, the saturated water content curves of both will present a crossover phenomenon, and this crossover phenomenon is more obvious with the increase of water content.

3.4. Quantitative analysis of micropore characteristics

Fig. 8a summarizes the pore size distribution of soil samples subjected to F-T cycles under the same dry density and water content conditions, and the pore diameter corresponding to the peak point in the curve is the most likely pore diameter. The soil samples with 13% moisture content and 1.48 g cm^{-3} dry density had more ultra-micropores (<0.05 μm) and micropores (0.05-2 μm) and less macropores (≥20 μm) after F-T cycles, but the results were higher than those of the soil samples without freezing-thawing cycle (N=0). We found that the peak value of pore size distribution curve shifts to the right and increases with the freeze-thaw cycle. After 10 F-T cycles, the curve presents a bimodal distribution, and the pore size distribution of the second peak is more than 10 μm. When the freeze-thaw cycle reaches 15 times (E1), the peak value reaches the highest, and the porosity reaches 32.39% (Fig. 8b). Although the peak value of F1 is lower than that of E1, it is still significantly higher than that of A1. Among them, the first peak of E1 was 19.40% and 14.93% less than that of D1 and F1. The second peak was 6.25% and 13.33% higher than D1 and F1, respectively. This indicates that the second peak in the pore diameter distribution curve plays a decisive role after 10 F-T cycles. The distribution curves of D1 and F1 approximately coincide, and the porosity difference between them is less than 3%, which is consistent with the result of saturated

286 water conductivity.

287 Fig. 9 shows the influence of water content and dry density on pore size
288 distribution of soil samples. With the increase of soil water content, the dominant pore
289 size moved to the right, gradually changing from micropores (0.05-2μm) to pores (2-
290 10μm), and the content increased. On the contrary, the distribution of dominant pore
291 size is not affected by the change of dry density, and the content will decrease with the
292 increase of soil dry density. When the dry density increases from 1.48 g cm^{-3} to 1.58 g
293 cm^{-3}, the first peak and second peak of dominant pore size decrease by 36.75% and
294 13.25% respectively. These results indicate that the K_s of soil is closely related to its
295 microstructure, while water content and dry density also affect the microstructure of
296 soil samples after F-T cycles to varying degrees, and thus affect the K_s of soil.

297 # 4. Discussion

298 We speculate that the degradation of permeability of saline-alkali soil is closely
299 related to its microstructure. Therefore, the saturated water conductivity test of soil was
300 carried out, and PSD, XRD, MIP and other advanced technologies were adopted to
301 study the microstructure of saline-alkali soil. The relationship between microstructure
302 and permeability of saline-alkali soil after freeze-thaw cycle was analyzed in order to
303 provide a theoretical basis for the restoration of microstructure of saline-alkali soil.

304 ## 4.1. Particle composition and mineral composition of saline-alkali soil based on
305 PSD and XRD

306 Soil particle composition is an important factor determining soil structure
307 characteristics[49].The distribution and texture of soil particle size directly affect the basic

physical properties of soil, especially the water absorption capacity of soil[50]. The mineral composition of the soil is also one of the important factors affecting the soil permeability. The high proportion of clay and clay minerals will reduce the soil permeability due to their hydrophilicity[14, 20, 51]. Our research data show that clay (particle size <0.002 mm) only accounts for 4.95% in saline-alkali soil, and the proportion of clay minerals is 9.55%, both of which account for less than 10% of the total proportion. Therefore, we can conclude that the grain size distribution and mineral composition are not the main reasons for the poor soil permeability in this region. Thus, MIP analysis is very necessary in our research.

4.2. Saturated hydraulic conductivity of saline-alkali soil based on Freeze-thaw cycling experiments

The freeze-thaw cycle is a process of energy input and output[52], in which the transport of water and salt will lead to changes in soil grain size and structure[49]. The degree of soil weathering by freezing is related to the number of freeze-thaw cycles and water content. After the initial freeze-thaw cycles, the crushing of coarse particles and the aggregation of fine particles in the soil will lead to a significant increase in porosity. After more freeze-thaw cycles, the soil structure will gradually aggregate and the particle size distribution tends to be stable[25, 49]. According to the local daily freezing and thawing times, we set a total of 6 freeze-thaw cycles (including N=0). It was found that the soil permeability coefficient increased non-linearly with the increase of the number of cycles. The reason is that ice lenses gradually form during freezing, and ice melts in the frozen soil during thawing, creating cavities that act as channels and

increase soil permeability[53]. When the number of F-T cycles reaches 15 times, it reaches the peak value. Compared with N=0, the K_s increases by 209.77%.

The initial porosity of soil plays a decisive role before F-T cycles[25], and the initial dry density of soil affects the initial porosity. Water to ice produces a volume change of about 9%, which affects the volume expansion of the pores during freezing[54]. Therefore, according to the standard compaction test, we determined the maximum dry density of the saline-alkali soil of 1.58 g cm^{-3} and the optimal water content of 16%, and the floating value can meet the conditions of the test area coverage. After the F-T cycles, soil is coupled by salt heave and frost heave, and soil pores change, resulting in more internal seepage channels, which means that soil porosity is the main influencing factor leading to the change of saturated water content. Freeze-thaw soils with high water content produce more expansive ice, which breaks the bonds between particles, in contrast, when soil water content is low, ice crystals only grow in soil pores[55-56]. This is consistent with our research results, the K_s of soil is significantly affected by changes in dry density and water content. Among them, compared with B7 and B9, C7 and C9, D7 and D9, E7 and E9, and F7 and F9, the K_s decreased by 42.25%, 53.52%, 57.36%, 49.80% and 41.15% respectively. Compared with B7 and B1, C7 and C1, D7 and D1, E7 and E1, and F7 and F1, the K_s increased by 17.0 %, 22.57%, 7.83%, 9.26% and 24.07% respectively. In addition, it has been shown that external stress of up to 2 MPa can be generated during soil freezing[57], Under the action of contact stress, the joints and frozen water in the soil will continue to grow and expand. As the circulation goes on, the growing ice crystals will produce pressure on the surface of the adjacent matrix

and reduce the internal porosity of the soil[58]. Therefore, when the F-T cycle reaches 20 times, the K_s of the soil decreases instead. At the same time, the formation of ice-penetrating crystals increases the pore water pressure, compressing the soil, which in turn increases the pore water pressure. During the F-T cycle test, the soil was always inside the constraint ring, and with the increase of soil internal pressure, the constraint of the ring on the soil was strengthened. Considering that high water content promotes frost heave, this explains the crossover in the saturation conductivity curve.

4.3. Pore size distribution of saline-alkali soil based on MIP after freeze-thaw cycles

Soil structure is an important factor affecting water conductivity[59-61]. The poor structure of saline-alkali soil is closely related to the low water conductivity and permeability of soil[62], these are consistent with our experimental results. Soil microstructure is closely related to its K_s and is strongly affected by freeze-thaw cycles. In the test, A1, A2 and A3, as soil samples without freeze-thaw cycles, have porosity of only 6.19-11.51%. The low porosity resulted in the low saturated water conductivity of the soil sample, which was only 1.48×10^{-5} cm/s. This makes it difficult for agricultural irrigation water to penetrate the soil, and the remaining water forms surface runoff, which accelerates soil nutrient loss. In addition, the dense soil structure and low porosity promoted soil capillarity in the floodplain of southwestern Shandong Province, and the salt remained on the surface with the evaporation of water after the rise of groundwater, which was extremely unfavorable to the development of agricultural production.

The MIP results showed that there were a lot of ultra-micropores in the soil samples in this area. However, more ultra-micropores in the soil were not conducive to the remediation of saline-alkali soil[48]. The F-T cycle can reduce the content of ultra-micropores and micropores in soil samples. After 10 F-T cycles, a new peak value appears at 10 μm, indicating that freeze-thaw cycles have a strong effect on soil macropores. Water content and dry density have great influences on F-T cycle. The water transport process becomes more complex under freeze-thaw cycles, and the complexity increases with the increase of water content. In the soil sample, the water was almost completely frozen into ice during the freezing process, and the soil particles were displaced due to volume expansion, and the soil particles were not completely restored to the original position during thawing[63], resulting in the deviation of the pore content and the increase of soil porosity. Therefore, we can determine that the increase of water content will shift the peak value of the curve to the right and increase the content of the intrusion volume, which is consistent with the results obtained from the saturated water conductivity test. In addition, the increase of dry density will strengthen the cementation between soil particles, and reduce the porosity in the soil. The growth of ice crystals and the formation of ice-penetrating crystals in the soil are further inhibited, and the intrusion volume of pores is correspondingly reduced, and the saturated water conductivity of the soil is reduced.

4.4. Effect of freeze-thaw cycles on salt discharge in saline-alkali soil

In recent years, some scholars have tried to change the microstructure of saline-alkali soil with different ameliorants[64]. On this basis, we try to find a new ameliorating

measure of saline-alkali soil. The former proposed that high soil porosity would improve its permeability[65], and our research supports this view. The results show that the appropriate freeze-thaw cycle can greatly improve the pore distribution, soil porosity and saturated water conductivity of saline-alkali soil in the southwest of Shandong Province. This is also due to the weak internal cohesion of natural saline-alkali soil, and irreversible plastic deformation will occur after several times of frost heave, which will not be affected by the change of salt content. In a certain range, the increase of water content can enhance the effect of freeze-thaw cycle. Considering the natural water content of 14.07% and the optimal water content of 16% in the experimental area, this idea is feasible.

The extreme temperature in winter reaches -16.5 °C in the Yellow Flood area of Southwest Shandong Province, which is a seasonal frozen soil area. Soil samples were taken from the topsoil layer (0-25 cm), which is included within the freezing depth of the soil in the area. Therefore, the F-T cycles can significantly improve the pore distribution and microstructure of crop surface soil. It is well known that after soil moisture evaporates, most of the salt and alkali remain in the surface of the soil[51], which requires that we need to broaden the channels of water circulation in the soil and let the salt go with the water. Therefore, we can take the freeze-thaw cycle as the basis for the salt discharge in the saline-alkali soil project in this area. Based on the above research, in order to achieve the effect of improving the local soil microstructure and considering the influence of dry density on the pore distribution, we suggest that local farmers should properly plough the cultivated land in winter. Besides, burette can be used to

418 increase the soil water content, in order to achieve the effect of promoting the freezing
419 and thawing cycle.

420 **5. Conclusions**

421 The existence of saline-alkali soil seriously endangers the agricultural production
422 and development in the floodplain of southwest Shandong Province. In this experiment,
423 MIP and SHC test were used to explore the relationship between soil microstructure
424 characteristics and K_s under F-T cycles. The main reason of low permeability of saline-
425 alkali soil is not the influence of grain size distribution and mineral composition. The
426 low permeability of surface saline-alkali soil is closely related to its microstructure, and
427 its pores are mainly composed of ultra-micropores and micropores. Under the action of
428 F-T cycles, soil pores transition from micropores and ultra-micropores to small pores.
429 When N=10, mesopore particles begin to be broken, and such fragmentation is the most
430 obvious when N=15, which is consistent with the law presented by soil saturated
431 hydraulic conductivity curve. High water content can improve the crushing effect of
432 freeze-thaw cycle on soil particles, and then improve soil permeability, while the
433 increase of dry density will play a certain inhibiting role. The results show that the
434 permeability of saline-alkali soil is closely related to its microstructure, and the freeze-
435 thaw cycle can improve the microstructure of saline-alkali soil to further improve its
436 permeability, which provides a certain reference direction for the restoration of saline-
437 alkali soil. Although the relationship between the microstructure of saline-alkali soil
438 and the saturated hydraulic conductivity has been comprehensively analyzed by various
439 methods in this experiment, there are still some limitations. In future studies, we need

to consider the restoration effects of F-T cycles on other soil textures, and consider the coupling effects of F-T cycles on salt content, temperature and other factors in combination with soil microstructure.

Data Availability

The data used to support the findings of this study are included within the article.

Acknowledgements

We gratefully acknowledge the public service sector special funds from the National Natural Science Foundation of China (project number: 51574156) and the Key Development Program for Research of Shandong Province (project number: 2018GNC110023).

Funding

Key Development Program for Research of Shandong Province, Grant/Award Number. 2018GNC110023; National Natural Science Foundation of China, Grant/Award Number: 51574156.

References

1. Qadir, M., Noble, A. D., Schubert, S., Thomas, R.J. & Arslan, A. Sodicity-induced land degradation and its sustainable management: problems and prospects. *Land Degradation & Development*. **17,** 661–676 (2006).

2. Xia, J. B., Ren, J. Y., Zhang, S. Y., Wang, Y. H. & Fang, Y. Forest and grass composite patterns improve the soil quality in the coastal saline-alkali land of the Yellow River Delta, China. *Geoderma.* **349,** 25–35 (2019).

3. Wang, S. J., Chen, Q., Li, Y., Zhuo, Y.Q. & Xu, L. Z. Research on saline-alkali soil amelioration

462 with FGD gypsum. *Resources Conservation and Recycling*. **121,** 82–92 (2017).

463 4. Qadir, M., Tubeileh, A., Akhtar, J. et al. Productivity enhancement of salt-affected environments

464 through crop diversification. *Land Degradation & Development.* **19,** 429–453 (2008).

465 5. Luo, S., Tian, L., Chang, C. L., Wang, S.J. & Zhang, J. F. Grass and maize vegetation systems

466 restore salinesodic soils in the Songnen Plain of northeast China. *Land Degradation & Development*.

467 **29,** 1107–1119 (2018b).

468 6. Zhou, R., Li, Y., Wu J. et al. Need to link river management with estuarine wetland conservation:

469 a case study in the Yellow River Delta, China. *Ocean Coast Management.* **146,** 43–49 (2017).

470 7. Qadir, M. & Schubert, S. Degradation processes and nutrient constraints in sodic soils. *Land*

471 *Degradation & Development*. **13,** 275–294 (2002).

472 8. Murtaza, B., Murtaza, G., Imran, M. et al. Yield and nitrogen use efficiency of rice-wheat

473 cropping system in gypsum amended saline-sodic soil. *Journal of Soil Science and Plant*

474 *Nutrition*.**17,** 686–701 (2017).

475 9. Temiz, C. & Cayci. G. The effects of gypsum and mulch applications on reclamation parameters

476 and physical properties of an alkali soil. *Environmental Monitoring and Assessment*. **190,** 347–358

477 (2018).

478 10. Sun, J. N., Yang, R. Y., Li, W. X. et al. Effect of biochar amendment on water infiltration in a

479 coastal saline soil. *Journal of Soils and Sediments*. **18,** 3271–3279 (2018).

480 11. Sakai, Y., Shimizu, C., Murata, H., Seto, H. & Wang, C. Changes in Soil Physicochemical

481 Properties and Maize Production Following Improvement of Salt-Affected Soils Using Coal Bio-

482 Briquette Ash in Northeast China. *Agronomy*, **10,** 348 (2020).

483 12. Wang, S.J., Chen, C. H., Xu, X. C. & Li, Y. J. Amelioration of alkali soil using flue gas

484 desulfurization by products: productivity and environmental quality. *Environmental Pollution*. **151,**
485 200-204 (2008).
486 13. Pandey, V. C., Abhilash, P. C. & Singh, N. The Indian perspective of utilizing fly ash in
487 phytoremediation, phytomanagement and biomass production. *Journal of Environmental*
488 *Managemen*t. **90,** 2943–2958 (2009).
489 14. Mao, W. B., Kang, S. Z., Wan, Y. S. et al. Yellow River sediment as a soil amendment for
490 amelioration of saline land in the Yellow River Delta. *Land Degradation & Development*. **27,** 1595–
491 1602 (2016).
492 15. Shandong Provincial Information Network. Natural Resources Database [EB/OL] (2020)
493 http://lib.sdsqw.cn/ftr/ftr.htm
494 16. Jia, J., Xie, X. L. & Yang, K. Soil microstructure evolution and macro deformation mechanism
495 for controlling construction disturbance in Shanghai soft soil. *Journal of Shanghai Jiaotong*
496 *University (Science)*. **21,** 713–718 (2016).
497 17. Kong, L. W., Wang, M., Guo, A. G. & Wang, Y. Effect of drying environment on engineering
498 properties of an expansive soil and its microstructure. *Journal of Mountain Science*. **14,** 1194–1201
499 (2017).
500 18. Tian, H. H., Wei, C. F. & Tan, L. Effect of freezing-thawing cycles on the microstructure of soils:
501 A two-dimensional NMR relaxation analysis. *Cold Regions Science and Technology*. **158,** 106–116
502 (2019).
503 19. Liu, J. Y. & Zhang, L. J. The Microstructure Characters of Saline Soil in Qarhan Salt Lake Area
504 and Its Behaviors of Mechanics and Compressive Strength. *Arabian Journal for Science and*
505 *Engineering*. **39,** 8649-8658 (2014).

20. Zhang, X. W. & Kong, L. W. Study of pore characteristics of offshore clay by SEM and MIP and NA methods. *Rock and Soil Mechanics*. **34,** 134–142 (2013).

21. Jha, A. K. & Sivapullaiah, P. V. Volume change behavior of lime treated gypsous soil - influence of mineralogy and microstructure. *Applied Clay Science*. **119,** 202–212 (2016).

22. Enrique & Romero. A microstructural insight into compacted clayey soils and their hydraulic properties. *Engineering Geology*. **165,** 3-19 (2013).

23. Deng, Y. F., Yue, X. B., Liu, S. Y., Chen, Y. G. & Zhang, D. W. Hydraulic conductivity of cement-stabilized marine clay with metakaolin and its correlation with pore size distribution. *Engineering Geology*. **193,** 146-152 (2015).

24. Geng, Y. H., Liu, C. X., LI, K. S. & Li, Q. X. Analysis of relationship between soil structure characteristics and permeability of silty saline-alkali soil in Yellow River Delta. *Water Saving Irrigation*. **2,** 27-31+36 (2020).

25. Xu, J., Li, Y., Ren, C. & Chen, G. Influence of freeze-thaw cycles on microstructure and hydraulic conductivity of saline intact loess. *Cold Regions Science and Technology*. **181,** 103183 (2021).

26. Han, Y., Wang, Q. & Xia, W. T. Experimental study on the hydraulic conductivity of unsaturated dispersive soil with different salinities subjected to freeze-thaw. *Journal of Hydrology*. **583,** 124297 (2020).

27. Ma, Q., Zhang, K., Jabro, J. D., Ren, L. & Liu H. Freeze–thaw cycles effects on soil physical properties under different degraded conditions in Northeast China. *Environmental Earth Sciences*. **78,** 1-12 (2019).

28. Liu, Y., Wang, Q., Liu, S. et al. Experimental investigation of the geotechnical properties and

528 microstructure of lime-stabilized saline soils under freeze-thaw cycling. *Cold Regions Science &*
529 *Technology*. **161,** 32-42 (2019).
530 29. Wang, T. H., Lu, J. & Zhang, J. F. Experimental study on permeability coefficient of artificially
531 compacted unsaturated loess considering influence of density. *Chinese Journal of Rock Mechanics*
532 *and Engineering*. **25,** 2364-2368 (2006).
533 30. Xu, J., Wang, Z. Q., Ren, Q. W. & Yuan, J. Experimental analysis on permeability law of
534 remolded loess under freezing-thawing condition. *Journal of Northwest A&F University (Natural*
535 *Science Edition)*. **45,** 134-142 (2017).
536 31. Wang, S., Ding, J., Xu, J., Ren, J. & Yang, Y. Shear Strength Behavior of Coarse-Grained Saline
537 Soils after Freeze-Thaw. *KSCE Journal of Civil Engineering*. **6,** 2437-2452 (2019).
538 32. Abdulrahman A., Marwen B. &Muzahim A. Impact of freeze–thaw cycles on mechanical
539 behaviour of lime stabilized gypseous soils. *Cold Regions Science & Technology.* **99**, 38-45 (2014).
540 33. Ministry of Water Resources of the People's Republic of China. GB50487-2008 Code for
541 engineering geological investigation of water resources and hydropower. 1rd ed. (*China Planning*
542 *Press; Beijing* (2009))
543 34. Kimpe, D. C. R. Effect of air-drying and critical point drying on the porosity of clay soils.
544 *Canadian Geotechnical Journal*. **21,** 181–185 (1984).
545 35. Delage, P. & Lefebvre, G. Study of the structure of a sensitive champlain clay and of its evolution
546 during consolidation. *Canadian Geotechnical Journal*. **21,** 21–35 (1984).
547 36. Ou, J. Q., Huang, W. H., Lu, Y. et al. Clay Mineral Composition and Spatial Distribution of
548 Stagnic Anthosols in Guangxi. *Soil*. **52,** 1290-1297 (2020).
549 37. Lin, B. T., Cerato, A. B., Madden, A. S. & Madden, M. E. E. Effect of fly ash on the mechanical

550 behavior of expansive soils: microscopic analysis. *Environmental & Engineering Geoscience*. **19,**
551 85–94 (2013).
552 38. Qi, J. L., Zhang, J. M. & Zhu, Y. L. Influence of freezing-thawing on soil structure and its soil
553 mechanics significance. Chinese. Journal of Rock Mechanics and Engineering. **22,** 2690－2694
554 (2003).
555 39. Lionel, C. W. & Moir, D. H. Cyclical closed-system freeze-thaw permeability testing of soil
556 liner and cover materials. *International Journal of Rock Mechanics and Mining Sciences*. **28,** 784-
557 793 (1991).
558 40. Lim, T. J., Spokas, K. A., Feyereisen, G. & Novak, M. J. Predicting the impact of biochar
559 additions on soil hydraulic properties. *Chemosphere*. **142,** 136-144 (2016).
560 41. Dikinya, O., Hinz, C. & Aylmore, G. Dispersion and re-deposition of fine particles and their
561 effects on saturated hydraulic conductivity. *Soil Research*. **44,** 78-83 (2006).
562 42. The Ministry of Water Resources of the People's Republic of China GB /T 50123-1999, Standard
563 for Soil Test Method. (China Planning Press: Beijing (1999))
564 43. Hussain, R., Ghosh, K. K. & Ravi, K. Influence of biochar particle size on the hydraulic
565 conductivity of two different compacted engineered soils. *Biomass Conversion and Biorefinery*. **pp,**
566 1-11 (2020).
567 44. Washburn, E. W. Note on a Method of Determining the Distribution of Pore Sizes in a Porous
568 Material. *Proceedings of the National Academy of Sciences of the United States of America*. **7,** 115-
569 116 (1921).
570 45. Zhang, T., Cai, G., Liu, S. & Puappala, A. J. Engineering properties and microstructural
571 characteristics of foundation silt stabilized by lignin-based industrial by-product. *KSCE Journal of*

572 *Civil Engineering*. **20,** 2725-2736 (2016).

573 46. Shear, D. L., Olsen, H. W. & Nelson, K. R. Effects of desiccation on the hydraulic conductivity
574 versus void ratio relationship for a natural clay. *Washington DC: Transportation research record,*
575 *NRC National Academy Press*. **pp 1369,** 130–135 (1993).

576 47. Li, X. & Zhang, L. M. Characterization of dual-structure pore-size distribution of soil. *Canadian*
577 *Geotechnical Journal*. **46,**129–141 (2009).

578 48. Li, K. S., Li, Q. X., Geng, Y. H. & Liu, C. X. An evaluation of the effects of microstructural
579 characteristics and frost heave on the remediation of saline-alkali soils in the Yellow River Delta,
580 China. *Land Degradation & Development*. **32,** 1325-1337 (2020).

581 49. Zhang, T., Ma, W., Feng, W., Xiao, D. & Hou, X. Reconstruction of Soil Particle Composition
582 During Freeze-Thaw Cycling. A Review. *Pedosphere*. **26,** 167-179 (2016).

583 50. Osman, K. T. Soils: Principles, Properties and Management. *Soil Use and Management*. **29,** 607-
584 607 (2013).

585 51. Mao, W. B., Wan, Y. S., Sun, Y. X., Zheng, Q. K. & Qv, X. L. Applying dredged sediment
586 improves soil salinity environment and winter wheat production. *Communications in Soil Science*
587 *and Plant Analysis*. **49,** 1787–1794 (2018).

588 52. Li, S. X., Nan, Z. T. & Zhao, L. Impact of freezing and thawing on energy exchange between
589 the system and environment. *Journal of Glaciolgy and Geocryology*. **24,** 109–115 (2002).

590 53. Chamberlain, E. J. & Gow, A. J. Effect of freezing and thawing on the permeability and structure
591 of soils. *Engineering Geology*. **13,** 73–92 (1978).

592 54. Walder, J. S. & Hallet, B. The physical basis of frost weathering. Toward a more fundamental
593 and unified perspective. *Arctic and Alpine Research*. **18,** 27–32 (1986).

55. Bullock, M. S., Kemper, W. D. & Nelson, S. D. Soil cohesion as affected by freezing, water content, time and tillage. *Soil Science Society of America Journal*. **52,** 770–776 (1988).

56. Ferrick, M. G. & Gatto, L. W. Quantifying the effect of a freeze-thaw cycle on soil erosion: laboratory experiments. *Earth Surf Processes & Land*, **30,** 1305–1326 (2005).

57. Tsytovich, N. A. The Mechanics of Frozen Soils. (High School Press: Moscow (1973))

58. Taber, S. The mechanics of frost heaving. *Journal of Geology*. **38,** 303–317 (1930).

59. Li, X. A., Li, L. C., Song, Y. X. et al. Characterization of the mechanisms underlying loess collapsibility for land-creation project in Shaanxi Province. *Engineering Geology*. **249,** 77–88 (2019a).

60. Meng, J. & Li, X. A. Effects of carbonate on the structure and properties of loess and the corresponding mechanism: an experimental study of the Malan loess, Xi'an area, China. Bulletin *Engineering Geology and the Environment*. **78,** 4965–4976 (2019).

61. Xu, L. & Coop, M. R. Influence of structure on the behavior of a saturated clayey loess. *Canadian Geotechnical Journal*. **53,** 1026–1037 (2016).

62. Ben-Hur, M., Yolcu, G., Uysal, H., Lado, M. & Paz, A. Soil structure changes: aggregate size and soil texture effects on hydraulic conductivity under different saline and sodic conditions. *Australian Journal of Soil Research*. **47,** 688–696 (2009).

63. Wang, J. Q., Wang, Q., Kong, Y. Y., Han, Y. & Cheng, S. K. Analysis of the pore structure characteristics of freeze‐thawed saline soil with different salinities based on mercury intrusion porosimetry. *Environmental Earth Sciences*. **79,** (2020) http://doi.org/10.1007/s12665-020-08903-w

64. Zhang, J. H., Bai, Z. G., Huang, J. et al. Biochar alleviated the salt stress of induced saline paddy

616 soil and improved the biochemical characteristics of rice seedlings differing in salt tolerance. *Soil*
617 *& Tillage Research*. **195,** 104372 (2019).
618 65. Ajayi A.E., Holthusen D. & Horn R. Changes in microstructural behaviour and hydraulic
619 functions of biochar amended soils. *Soil & Tillage Research*. **155**, 166–175 (2016).

Figures

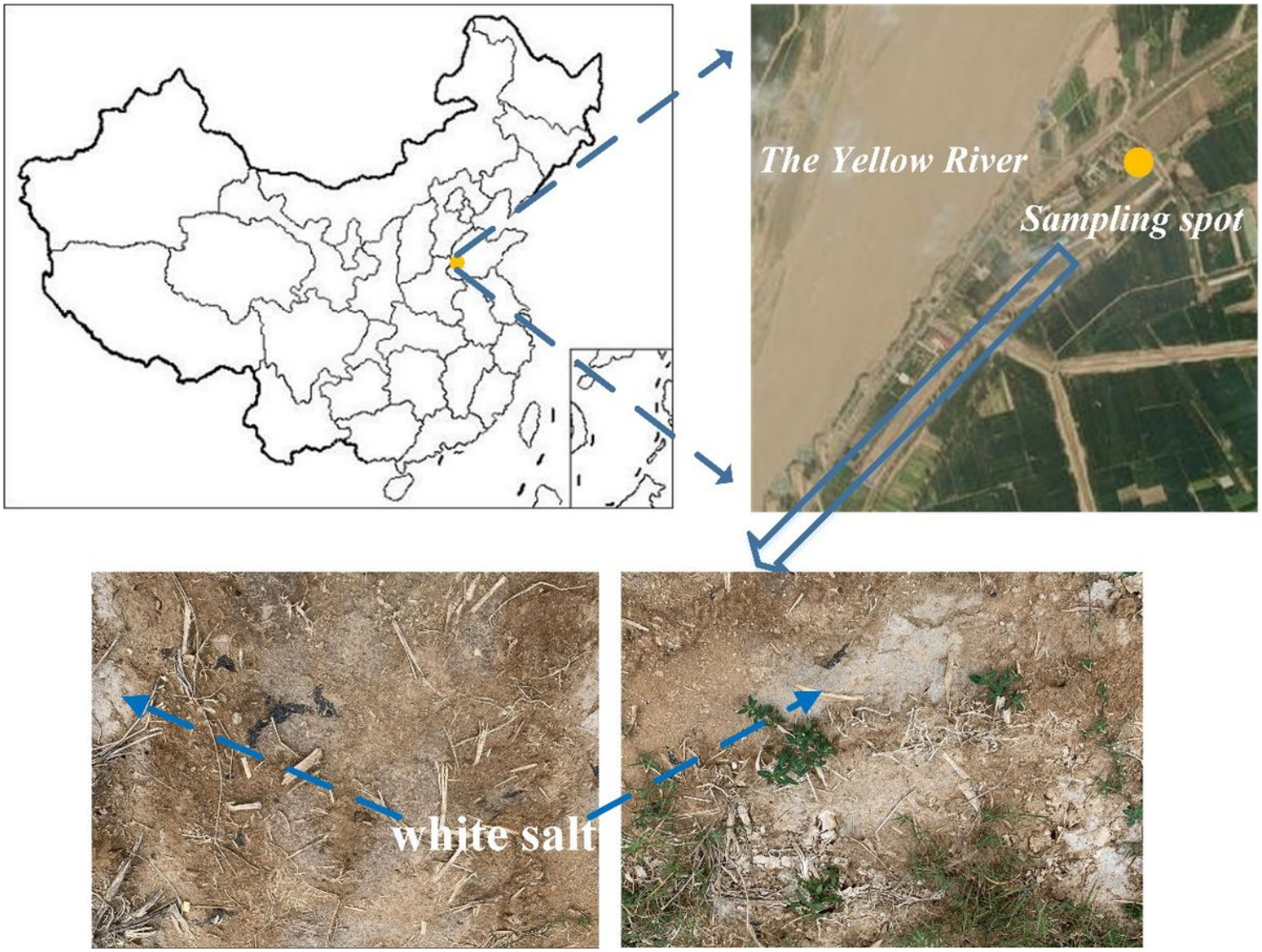

Figure 1

Study area and sampling location.

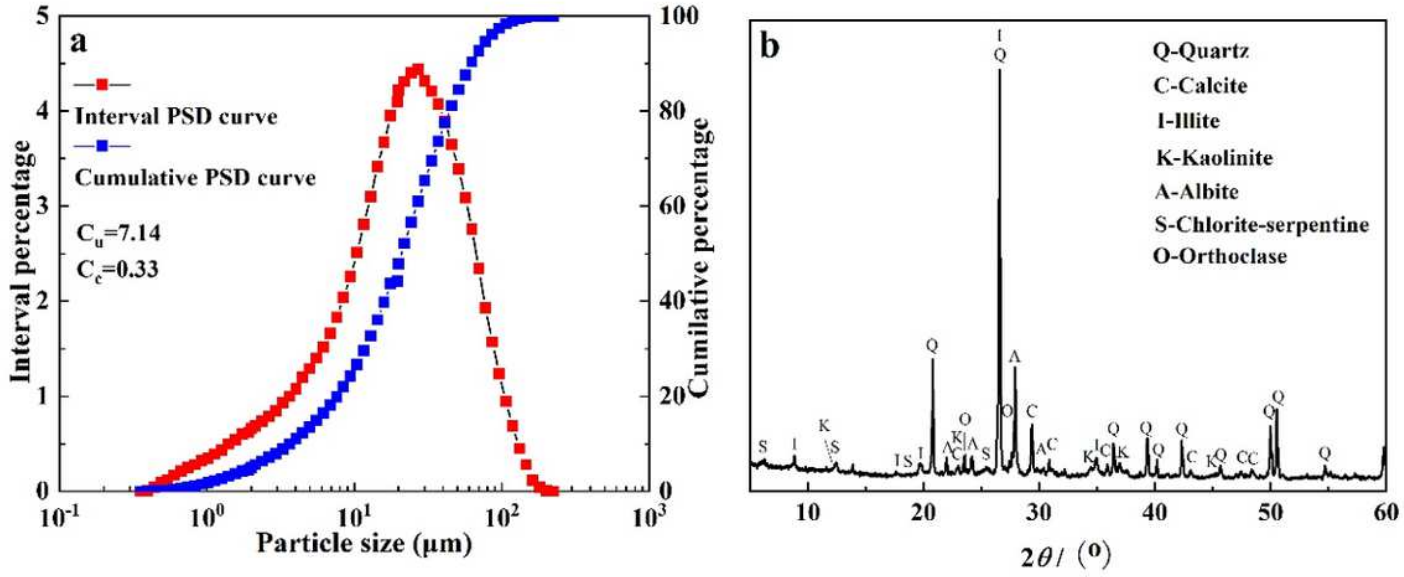

Figure 2

PSD curves and XRD curves of saline-alkali soils in the floodplain of southwestern Shandong Province: a particle size distribution cures b X-ray diffraction pattern.

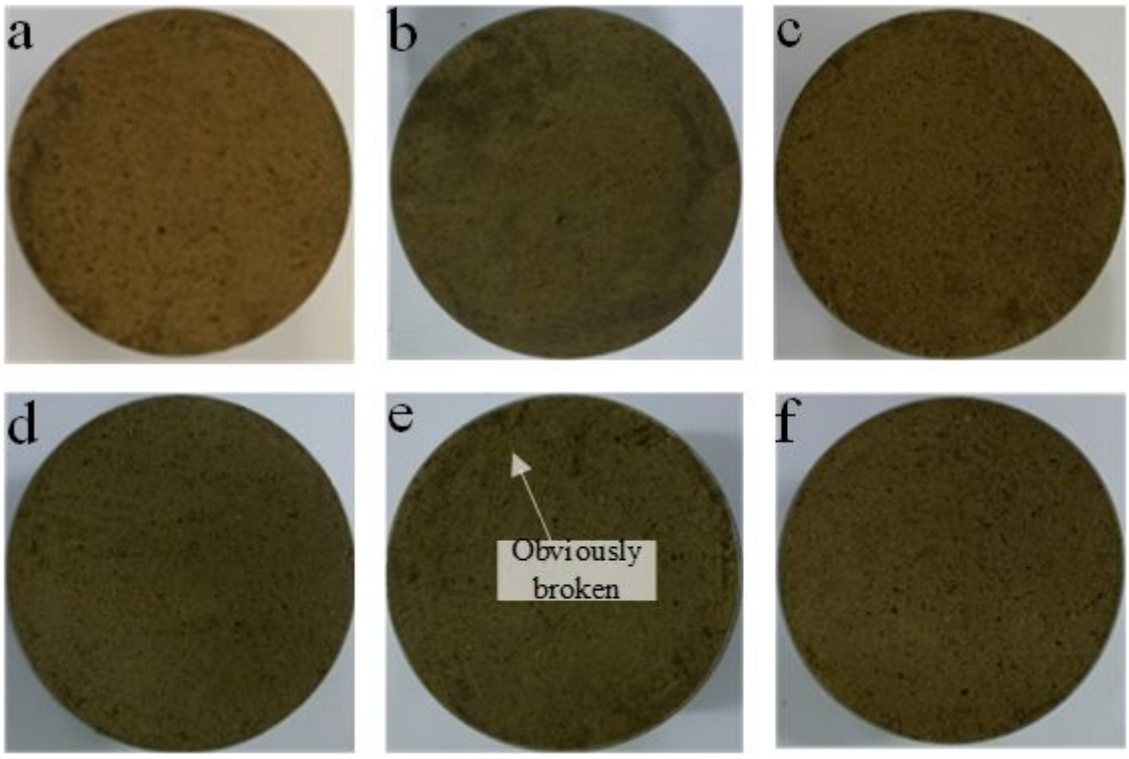

Figure 3

Soil samples with a moisture content of 13%, 1.48 g cm-3 and different freeze-thaw cycles: a N=0, 13%, 1.48 g cm-3 b N=1, 13%, 1.48 g cm-3 c N=5, 13%, 1.48 g cm-3 d N=10, 13%, 1.48 g cm-3 e N=15, 13%, 1.48 g cm-3 f N=20, 13%, 1.48 g cm-3.

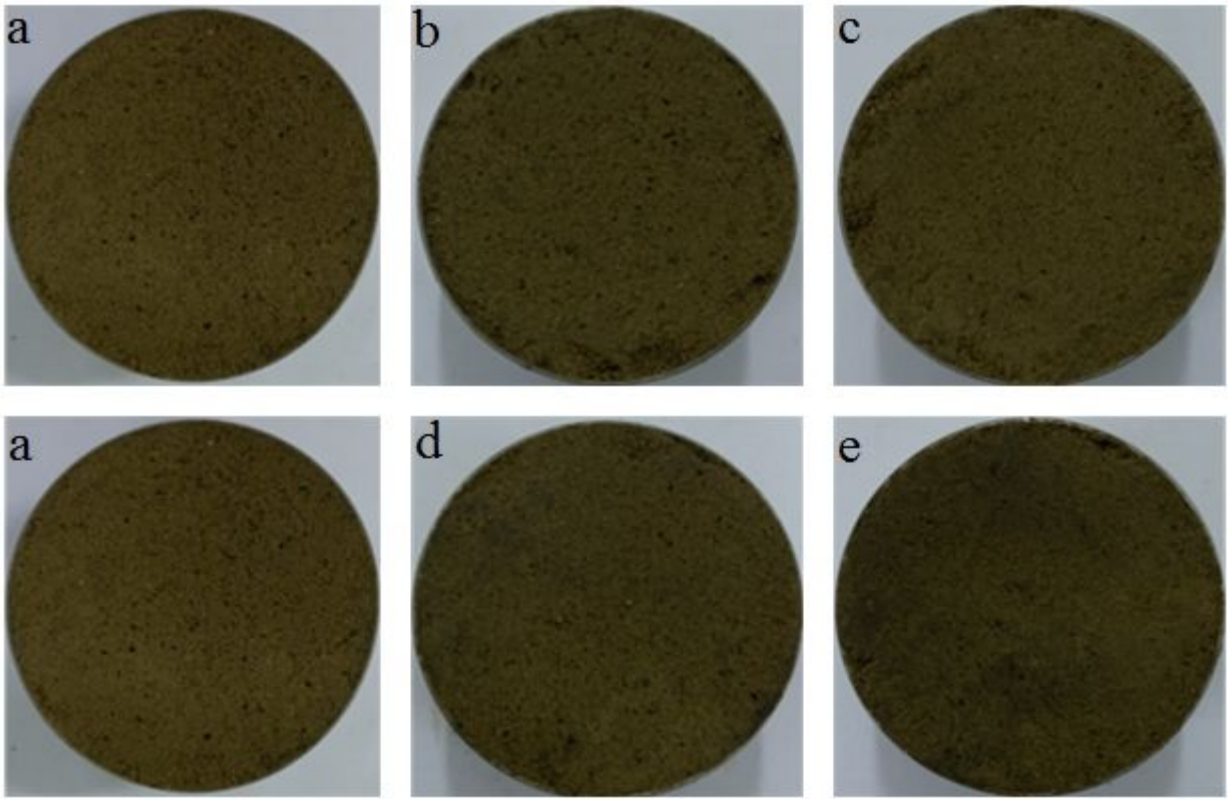

Figure 4

Soil samples affected by a single factor after 20 freeze-thaw cycles a N=20, 13%, 1.48 g cm-3 b N=20, 16%, 1.48 g cm-3 c N=20, 19%, 1.48 g cm-3 d N=20, 13%, 1.53 g cm-3 e N=20, 13%, 1.58 g cm-3.

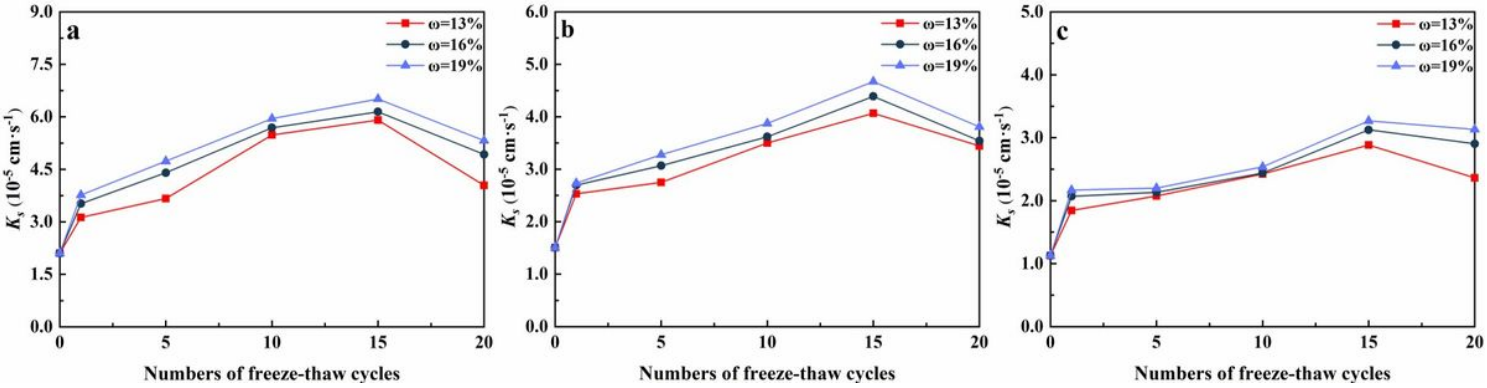

Figure 5

The changes of Ks of water-bearing remolded soils at the study site in the floodplain of southwestern Shandong Province caused by the changes of F-T cycles: a ρd=1.48 g cm-3 b ρd=1.53 g cm-3 c ρd=1.58 g cm-3.

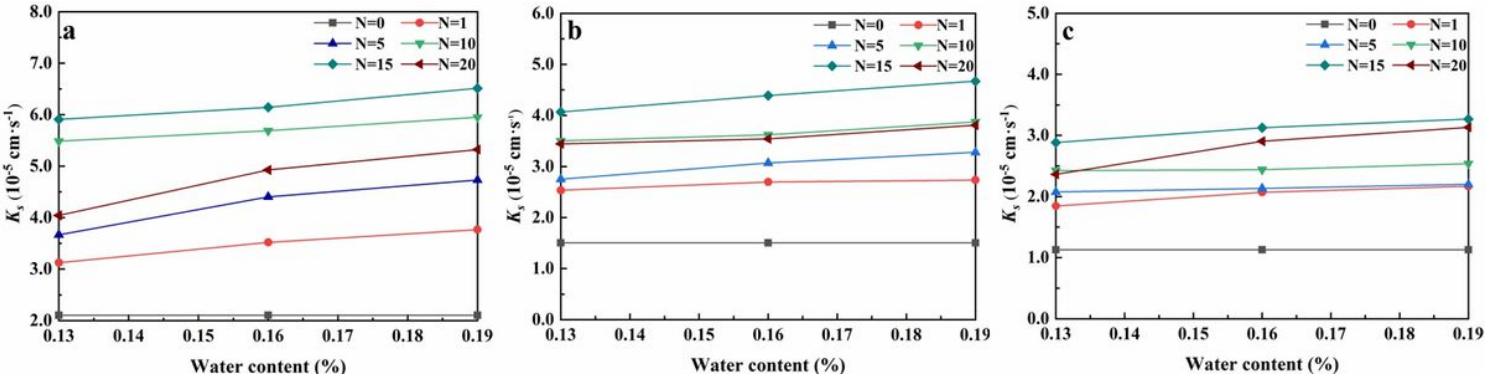

Figure 6

The changes of Ks with water content of water-remolded soils at the study site in the floodplain of southwestern Shandong Province: a ρd=1.48 g cm-3 b ρd=1.53 g cm-3 c ρd=1.58 g cm-3.

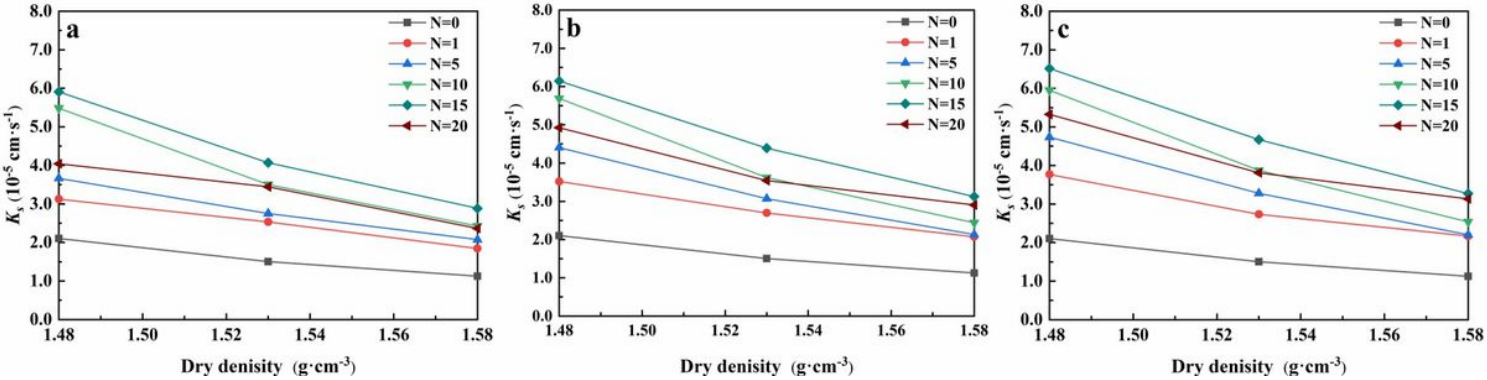

Figure 7

The changes of Ks with dry density of water-remolded saline-alkali soils at the study site in the floodplain of southwestern Shandong Province: a ω=13% b ω=16% c ω=19%.

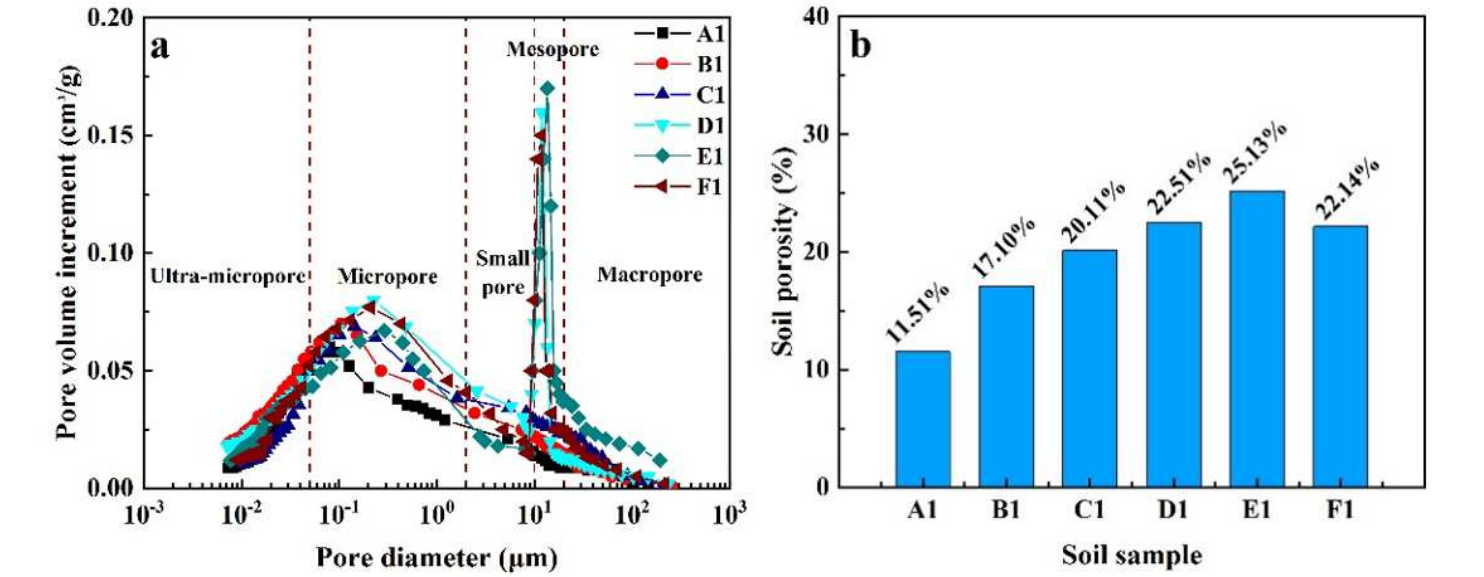

Figure 8

Pore-size distribution cures and bar chart of soil porosity distribution for soils at the study site in the floodplain of southwestern Shandong Province: a The water content is 13% and the dry density is 1.48 g cm-3, pore-size distribution curves with different F-T cycles b Bar chart of soil porosity distribution.

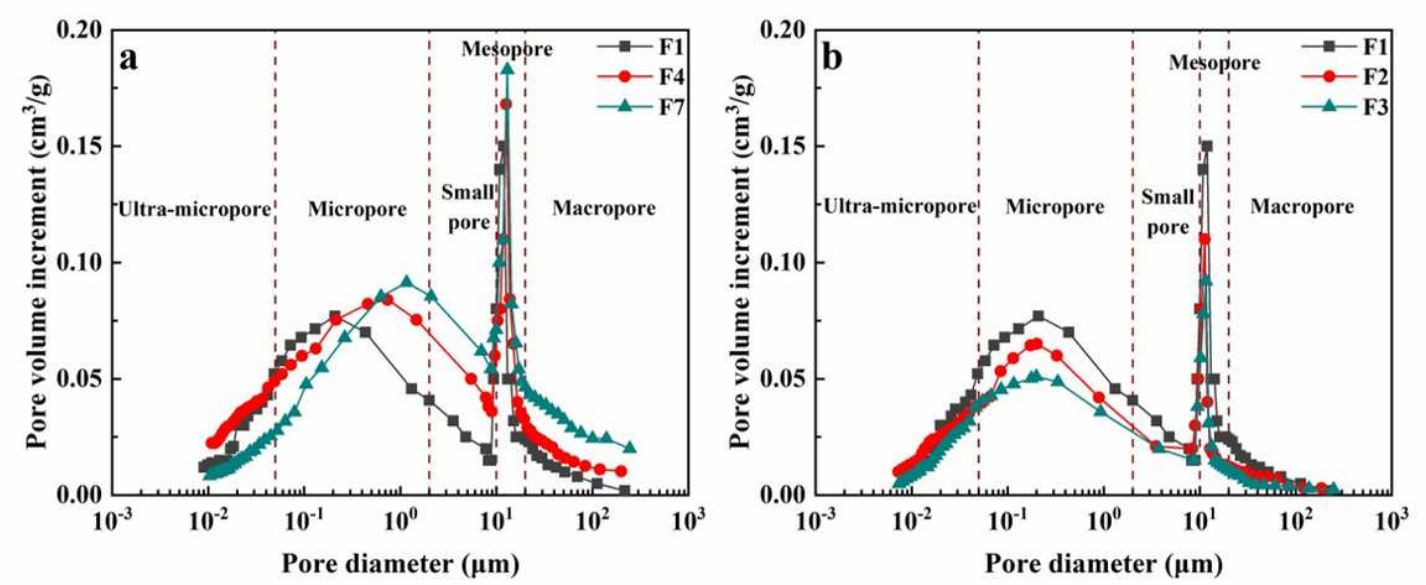

Figure 9

Pore-size distribution cures with different water content and dry density or soils at the study site in the floodplain of southwestern Shandong Province: a The dry density is 1.48 g cm-3, pore-size distribution cures with different water contents b The water content is 19%, pore-size distribution cures with different dry densities